# Combining Harmonic Laser Beams by Fiber Components for Refractivity–Compensating Two-Color Interferometry

Yang Liu, Anni Röse, Günther Prellinger, Paul Köchert, Jigui Zhu, and Florian Pollinger

***Abstract*—A perfect spatial overlap with multiple beams of different wavelengths is a prerequisite for multi–wavelength interferometry. Beam combination with the help of fibers seems to be an interesting method for this. We investigated three different types of fiber components, multi–mode wavelength division multiplexers (MM–WDMs), single–mode wavelength division multiplexers (SM–WDMs), and endlessly single–mode polarization maintaining photonic crystal fibers (PM–PCFs). All three seem potential candidates for a perfect spatial overlap of laser beams separated by an octave, i.e. fundamental and harmonic beams. We performed an experimental study on the impact of these components on polarization, wavefront, and coherence. These properties are essential for high–accuracy interferometry. As a test system, we used the fundamental and second harmonic beam of a Nd:YAG laser system at 1064 and 532 nm as a popular system in two–color interferometry for intrinsic refractive index compensation. The experimental results show the potential of PM–PCFs for this challenging application.**

***Index Terms*—Beam properties, photonics crystal fiber (PCF), two–color interferometry, wavelength division multiplexing (WDM).**

## I. Introduction

LARGE–SCALE distance measurement with a relative measurement uncertainty better than $10^{-6}$ is a current challenge in dimensional metrology. Highly accurate interferometric schemes have been developed in the last years for application in industrial engineering [1] or geodetic surveying [2], for example. Those measurements are performed under atmospheric rather than vacuum conditions and suffer from limitations imposed by the atmosphere: propagation of light rays, refraction errors, turbulence and changes of the refractive index of air [3]. The latter contributor usually limits the achievable measurement uncertainty and can be compensated by various techniques (sensor–based Edlén correction, refractometry, two–color interferometry) [4]–[6].

As a very flexible approach to this problem, two–color interferometers are used for inline refractive index compensation. The geometric path $l$ can be extracted from the measurement of the two optical paths $d_1$ and $d_2$ solely, by evaluating $l = d_1 - A(d_2 - d_1)$. The "*A*–factor" defined by $A = (n_1 - 1)/(n_2 - n_1)$ incorporates the refractive index correction, with $n_{1,2}$ representing the refractive indices. Inserting standard dispersion models shows that this $A$–factor does not depend on air pressure or temperature in the beam path [7], [8] in dry air, in a slightly extended formulation also in humid air [9]. This is exploited for intrinsic refractive index compensation. Unfortunately, any measurement uncertainty is mercilessly scaled up in the final result by the *A*–factor which depends on the measurement mode (group or phase velocity), and on the laser wavelengths used [6, chpt. 5.3]. It has a typical order of magnitude for optical and near–infrared systems between 20 and 160. To assure a fixed laser frequency ratio, two–color interferometry is frequently realized by the fundamental and second harmonic of a single laser source [10], [11]. The respective beams of a Nd:YAG laser source (1064 nm and 532 nm) span over a region of large dispersion. This implies a small *A* factor and makes this system specifically interesting for applications requiring intrinsic refractive index compensation [12]–[14].

One important source of measurement uncertainties limiting the accuracy of two–color interferometry and multi–wavelength interferometry, in general, are geometric errors. For straightforward interferometer designs, the initial overlap of fundamental and second harmonic can be maintained for the interferometric measurement [15]. In many cases, however, additional (e.g. acousto– or electro–optic) beam manipulation is necessary to achieve longer ranges of non–ambiguity or to realize particular modular system designs. State-of-the-art is the recombination of the two beams by a neutral beam splitter or a dichroic mirror (see e.g. [10], [14], [16]). Inevitably, this procedure leads to an imperfect superposition of the fundamental beams. This inherent cosine error is subsequently scaled up by the *A* factor. The need for a high–precision alignment with long–term stability

Manuscript received May 16, 2019; revised October 30, 2019 and November 29, 2019; accepted December 11, 2019. Date of publication December 18, 2019; date of current version April 1, 2020. This project has received funding from the EMPIR programme co-financed by the Participating States and from the European Union's Horizon 2020 research and innovation programme. Y. Liu acknowledges funding from the Chinese Scholarship Council (CSC) for his scientific stay in Germany. *(Corresponding author: Florian Pollinger.)*

Y. Liu is with the State Key Laboratory of Precision Measurement Technology and Instruments, Tianjin University, 300072 Tianjin, China, and on leave from the Physikalisch-Technische Bundesandstalt, 38116 Braunschweig, Germany (e-mail: liuyangly@tju.edu.cn).

A. Röse, G. Prellinger, P. Köchert, and F. Pollinger are with the Physikalisch–Technische Bundesanstalt, 38116 Braunschweig, Germany (e-mail: anni.roese@ptb.de; guenther.prellinger@ptb.de; paul.koechert@ptb.de; florian.pollinger@ptb.de).

J. Zhu is with the State Key Laboratory of Precision Measurement Technology and Instruments, Tianjin University, Tianjin 300072, China (e-mail: jiguizhu@tju.edu.cn).

Color versions of one or more of the figures in this article are available online at http://ieeexplore.ieee.org.

Digital Object Identifier 10.1109/JLT.2019.2960473

is one reason for the lacking broader commercial success of refractive–index–compensating two–color interferometers.

In principle, transmission through an identical fiber ensures almost perfect spatial overlap and beam orientation for different laser beams. However, a straightforward combination of the typical wideband laser beam pairs for multi–wavelength interferometry using simple standard fiber components destroys essential beam properties for laser interferometry. Transmission in classical broadband multi–mode fibers leads to distorted wavefronts at the output due to speckles, and thus loss of spatial coherence. Single–mode transmission is strictly limited by the cut–off wavelength with the single–mode fiber. However, modern wavelength division multiplexer systems (WDMs), either in single mode or even in multi–mode architecture (SM–WDMs or MM–WDMs, respectively) could provide a commercially interesting option if the transmitted beam properties met the requirements for laser interferometry. Beyond classical fibers, photonic crystal fibers (PCFs), also called microstructured fibers, have received increasing attention for endlessly single–mode operation [17], dispersion managing [18] and low bending loss [19]. The wideband wavelength division multiplexing (WDM) transmission has been successfully achieved with PCF for widespread applications, such as optical telecommunication [20]–[24], super–continuum source [25], fiber amplifier [26], physical sensor [27], and coupler fabrication [28], [29], for example.

To investigate these beam combination options for multi–wavelength interferometry, three commercial fiber components, an MM–WDM, an SM–WDM, and a combination scheme based on an endlessly single–mode polarization–maintaining photonic crystal fiber (PM–PCF) have been systematically investigated and compared to each other in this study. As a very popular two–color system, the fundamental and second harmonic wavelength (532 nm and 1064 nm) from a Nd:YAG laser were used. The focus of this study was on the three beam characteristics: polarization behavior, wavefront quality, and coherence. This paper is organized as follows. Section II describes the basic principle and coupling system using fiber components for combining the two–color beams. Sections III, IV and V present the experimental schemes and results for evaluation of the beams properties from three commercial fiber components. In Section VI, these results are jointly discussed and an optimum approach derived.

## II. Fiber–Assisted Beam Combination: Experimental Setup and Coupling Efficiencies

Wavelength division multiplexers (WDMs) seem a natural choice for the combination of two beams of different colors [30]. A common fabrication method is heatingly fusing the cores of fibers together over a length of a few millimeters, then inserting into a common fiber (or a splitter for multiple outputs) through evanescent power coupling in the fused region [31], [32]. For our purpose, they can be seen as a Y–coupler: the two input fibers of a WDM are designed for the two different wavelengths, while a suitable broadband– capable output fiber needs to be identified. For our study, we selected a commercial MM–WDM (TM200R5F1B, Thorlabs) which provides a broad bandwidth

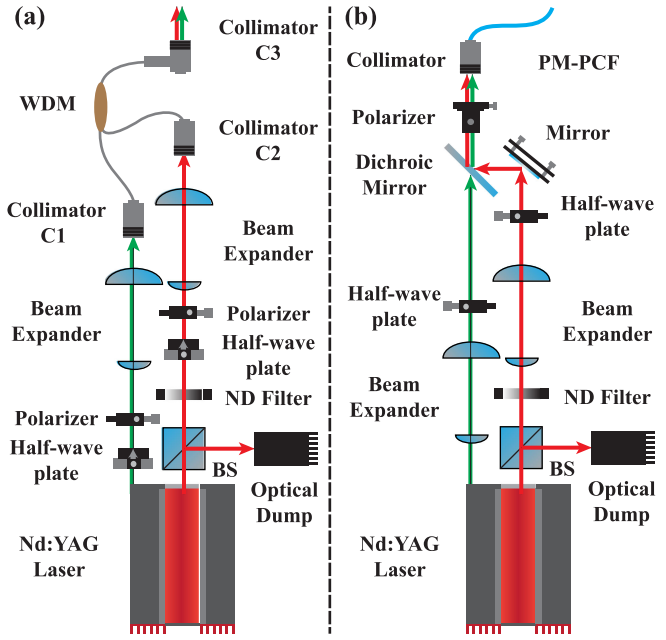


Fig. 1. Combination of two–color beams with fiber components. (a) WDM–based combination with WDM. (b) Combining system with endlessly single–mode PM–PCF. BS: beam splitter; ND filter: neutral density filter.

from 400 nm to 2200 nm. Both input and output port are terminated by FC/PC connectors. Two collimators (F280FC–A, Thorlabs, and F220FC–780, Thorlabs) are used for coupling the light into the MM–WDM. The SM–WDM combiner had been customized for this application (C08453981, LIGHTEL). The input fiber for 532 nm is an NUFERN 460HP, for the 1064 nm input and the joint output an OFS 980 FIBER were chosen. The length of the output fiber was restricted to 15 cm to confine the transmission of the 532 nm beam through the imperfect 1064 nm output fiber. The input ports are both terminated by FC/APC connectors and the output port by an FC/PC connector. Two collimators (F280APC–A, Thorlabs, and F280APC–C, Thorlabs) optimized for the APC termination are used for the input fibers.

Fig. 1(a) shows the simplified coupling system for combining the two beams emitted from a frequency–doubled Nd:YAG (Prometheus 20, Coherent) output beams with a WDM. The fundamental at 1064 nm is emitted with a power of up to 1 W, the second harmonic of up to 20 mW. The power of 1064 nm is divided by a beam splitter (BS041, Thorlabs). 90% of the primary intensity is blocked by an optical dump (BT600/M, Thorlabs). The intensity can be further adjusted by a variable neutral density filter (NDC–25C–2 M, Thorlabs). The beams at 532 nm and 1064 nm are each aligned by two mirrors (omitted in Fig. 1(a)) into beam expanders ($f_1 = 20$ mm and $f_2 = 80$ mm) which can be used to improve the coupling efficiency. Then the two beams are aligned by additional two mirrors for coupling into the WDM (omitted in Fig. 1(a)). Since PCF–based Y–couplers [28], [29] are not readily commercially available to our knowledge, we superposed the two beams by a dichroic mirror (DMSP805, Thorlabs) ex-situ, before coupling into a single–mode broadband PM–PCF (aeroGUIDE–5–PM, NKT

TABLE I
COUPLING EFFICIENCY OF THE THREE FIBER COMPONENTS

| Components | Wavelength (nm) | Input (mW) | Output (%) | After RC–08 (%) | After GT–10 (%) |
|---|---|---|---|---|---|
| MM–WDM | 532 | 1.91 | 42.7 | 24.3 | 8.4 |
| | 1064 | 1.65 | 42.4 | 22.1 | 8.5 |
| SM–WDM | 532 | 1.91 | 30.9 | 25.3 | 14.1 |
| | 1064 | 1.65 | 32.9 | 26.6 | 17.9 |
| PM–PCF | 532 | 2.19 | 64.4 | 58.5 | 52.7 |
| | 1064 | 2.50 | 28.7 | 22.6 | 19.3 |

Photonics) (cf. Fig. 1(b)). The input connector is terminated by FC/APC, and the output by FC/PC. The superposed two–color beams are coupled into the PCF by a collimator (F280APC–A, Thorlabs) mounted on a six–axis mount (K6XS, Thorlabs) to guarantee a fine and stable coupling. For the optimization of the coupling, an iterative procedure is performed, using the transmitted power for control. The spatial alignment is adjusted with the mirrors and the six axis mount by beam walking. Beam spot size and curvature can be adjusted by tweaking the beam expansion. Matching of the polarization can be fine-tuned with the wave plates and the input polarizer. The optimum polarization orientation defined by maximum polarization conservation is achieved when the output power after an analyzing polarizer is insensitive to beam bending (see also Section III).

In Table I, typical power efficiencies compared with the input power for the three coupling scenarios are compiled. The effective coupling efficiency was determined with a direct fiber connector on a commercial power meter (S120 C, Thorlabs). Because of its large core diameter (200 $\mu$m) the MM–WDM achieves the highest power transmission (42.7% for 532 nm, and 42.4% for 1064 nm), while the coupling efficiency for the SM–WDM is a bit lower (30.9% for 532 nm, and 32.9% for 1064 nm). The MM–WDM shows a relatively large insertion loss after the RC-08 collimator. Since the numerical aperture (NA) of the collimator does not perfectly match the NA of the MM–WDM, the beam is slightly truncated. In the case of the PM–PCF, a highly efficient coupling ratio is realized for 532 nm (64.4%) for which the collimator (F280APC–A, Thorlabs) is optimized. In the infrared, power efficiencies of approx. 29% can still be easily achieved. Thus, satisfactory coupling efficiencies can be achieved for all fiber–assisted superposition schemes investigated in this study.

## III. DEGREE AND STABILITY OF THE POLARIZATION

For interferometer applications, the mere coupling efficiency is an insufficient measure for the transmitted beam quality. As mentioned, in refractivity–compensated absolute interferometry, the effect of interferometer nonlinearities (typically in the range from 0.1 nm to 10 nm [33]) is scaled up with the $A$ factor and the uncertainty scaling induced by synthetic wavelength interferometry (e.g., at our setup [12] uncertainties are amplified by a factor 300 000 [12], [14]). Former research work [4], [34] has described several reasons for nonlinearities in

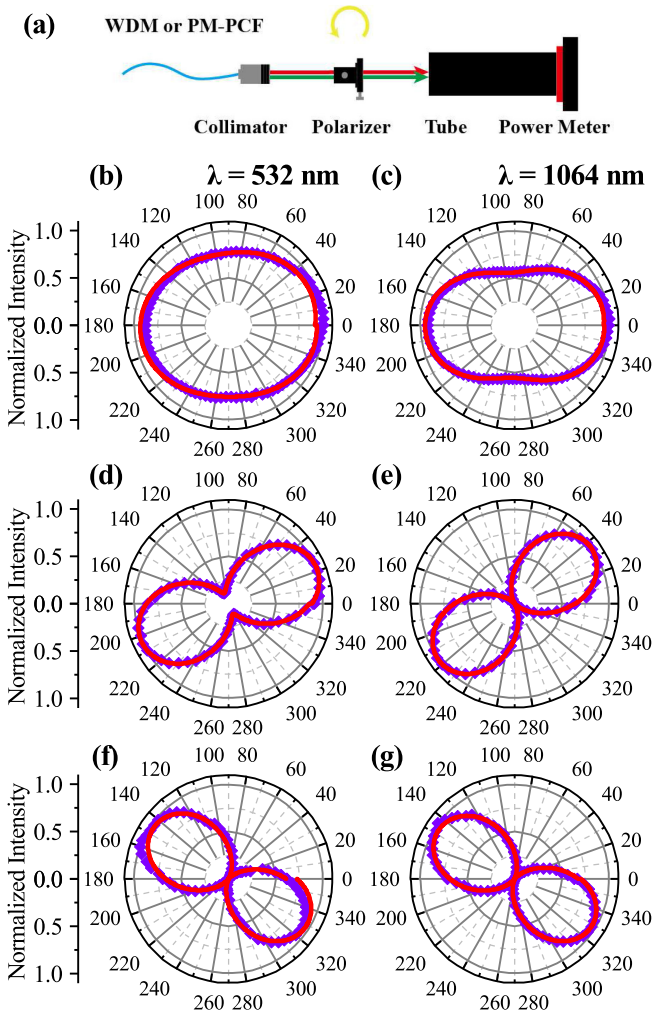


Fig. 2. Polarization measurements of two–color beams emitted from three fiber components. (a) Experimental setup, (b) and (c) polar coordinates and fitting plots for the MM–WDM, (d) and (e) polar coordinates and fitting plots for the SM–WDM, and (f) and (g) polar coordinates and fitting plots for the PM–PCF fiber.

displacement measuring interferometry which would go beyond the scope of this paper. However, if a polarization sensitive interferometer is fed by fiber, its nonlinearity characteristics are strongly influenced by the properties of this optical fiber [33], [35]. To define the polarization, interferometer heads often clean the entering polarization by a polarizer with high–polarization extinction following the collimation optics. We mimic this setup by a reflective collimator (here RC–08, Thorlabs), followed by a broadband Glan–Taylor polarizer (GT–10, Thorlabs). As mentioned in Section II, the RC–08 collimator chosen for its achromatic focal length for these experiments slightly truncates the beams emitted by the fibers. Table I shows that the usable intensity is significantly reduced after the following polarizer in case of the non–polarization maintaining WDM combiners, while the polarizer has a comparably negligible impact in case of the PM–PCF. The polarization of beams can be further studied by rotating the polarizer (here in steps of 4 degrees). In Fig. 2, the respective data is depicted in polar coordinates and fitting

TABLE II
EXPERIMENTAL ELLIPTICITY OF THE TRANSMITTED POLARIZATION

| Components | Wavelength (nm) | $DOP$ | $SOP(^\circ)$ | $PER$(dB) |
|---|---|---|---|---|
| MM–WDM | 532 | 0.14 | 40.98 | 1.22 |
| | 1064 | 0.28 | 36.86 | 2.50 |
| SM–WDM | 532 | 0.79 | 9.37 | 18.78 |
| | 1064 | 0.99 | 2.58 | 26.94 |
| PM–PCF | 532 | 0.99 | 3.34 | 24.69 |
| | 1064 | 0.99 | 3.91 | 23.32 |

plots with $\cos^2$ function (due to Malus' Law [36]). In Table II, the derived numerical values for the standard measures for comparing the ellipticity, degree of polarization ($DOP$) [37],

$$DOP = \frac{I_{\max} - I_{\min}}{I_{\max} + I_{\min}}, \tag{1}$$

state of polarization ($SOP$) [38],

$$SOP = \frac{180^\circ}{\pi} \times \arctan \sqrt{\frac{I_{\min}}{I_{\max}}}, \tag{2}$$

and percentage of extinction ratio ($PER$) [39],

$$PER = 10 \log \left( \frac{I_{\max}}{I_{\min}} \right) \tag{3}$$

are briefly summarized. These results support the increasing quality of polarization transmission from the MM–WDM over the SM–WDM to the PM–PCF. The results of the SM–WDM depend very strongly on the specifics of the fiber guidance, e.g. on the existence of small curvatures (see also the discussion below). While this general tendency might not be completely surprising, we want to stress the high quality of the polarization of both colors transmitted through the PM–PCF depicted in Fig. 2(f) and (g). Moreover, the fast axes are there almost identically oriented for both colors.

The application in practice as feed for a polarization sensitive interferometer requires a certain robustness of the polarization state towards external influences, in particular mechanical disturbances like bending, twisting, vibrations, caused, e.g., by ambient condition changes (pressure, temperature, sound). Otherwise, this may induce intensity fluctuations in a polarization sensitive interferometer. The polarization maintenance of the fiber is determined by its internal linear birefringence state, which is basically created during the fabrication process. External stress modifies the birefringence field and promotes mode conversion of the electromagnetic field. This leads to a changing birefringence behavior and results in so-called birefringent noise [35, chpt. 2.5]. In Fig. 3(a) and (b) the change in polarization under moderate stress is demonstrated for the PM–PCF and the SM-WDM. Kept straight, both fibers show nearly perfect polarization maintenance. Then, they are coiled up to a single fiber loop with a diameter of 6 cm. The PM–PCF polarization transmission is unaffected within the resolution limits of the experiment (Fig. 3(a)), while polarization orientation and degree are strongly altered in case of the SM–WDM (Fig. 3(b)). Fig. 3(c) demonstrates the impact on a simple Michelson set up

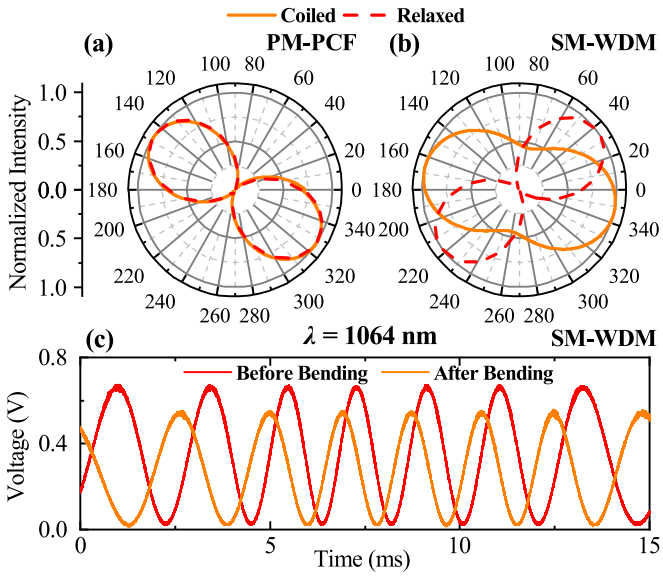


Fig. 3. Polarization–conservation under external stress. (a) and (b) Influence on the polarization degree when curling the PM-PCF (a) and the SM-WDM (b). The set-up is identical to Fig. 2(a). The polarization degree and orientation changes significantly for the SM-WDM. (c) Effect on the interference contrast of a polarization–sensitive Michelson–type interferometer.

following the output polarizer (see Section V). The interference contrast even of the 1064 nm signal, for which the SM transmission is optimized, changes significantly when slightly bending the fiber. Such amplitude fluctuations from the polarization or transmission mode can be misinterpreted as phase fluctuations if they are not suppressed by the detection scheme.

But there are also limitations in polarization maintenance of the PM–PCF. This can be seen if the external stress is increased and dynamically applied. To demonstrate this, we use a measurement setup following [33] (see Fig. 4(a)). The PM–PCF is coiled into multiple loops and inserted into a squeezer, resulting in a bending of the fiber. Additionally, we have extended the setup by using a piezo actuator (P–802.10, PI, and M–462, Newport) to shake the fiber coil with a sinusoidal modulation frequency from 130 Hz to 1.18 kHz. The modulation amplitude is changed between 2.5 V and 7.5 V, which is equivalent to a moving range of about 7.5 $\mu$m. The optical power of the two beams with different wavelengths after the polarizer is detected by unequal photodetectors (HCA–S–200M–SI and HCA–S–200M–IN, FEMTO). The noise spectra are evaluated by applying a Fast Fourier Transformation (FFT) method on the acquired data from an oscilloscope (SDS1104X–E, SIGLENT, Sampling rate: 10 MSa/s, and memory depth: 1.4 Mpts). They are processed offline. The results indicate that the polarization maintenance of the fiber varies with the excitation frequency similarly for both colors, with an increased sensitivity in the range around 200 to 600 Hz. This specific frequency certainly depends on the mechanical resonances of the whole set up. If a distinctly constant degree of polarization is required, suitable vibration isolation measures are hence necessary. To minimize the impact of the birefringent noise, AC–based detection schemes can be used in an interferometer design, for example. The resonance range is limited below 600 Hz for the PM–PCF investigated in

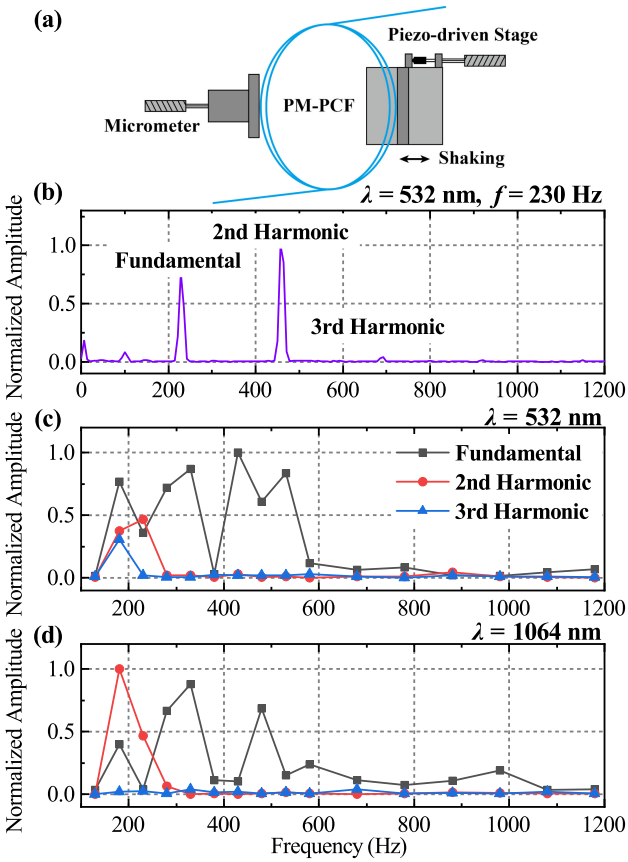


Fig. 4. (a) Fiber manipulator for noise test. (b) A typical FFT spectrum of noise with excitation. Resulting amplitude of the excitation frequency and its harmonics in the FFT spectrum of the transmitted power of the (c) 532 nm and (d) 1064 nm beams.

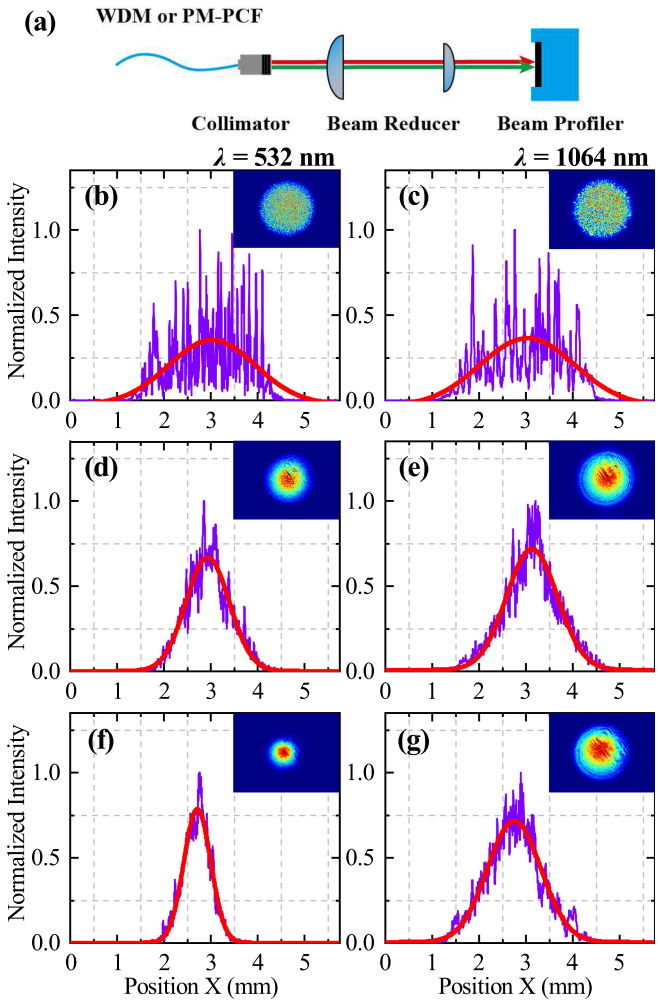


Fig. 5. The experimental results of beam profiles and their equatorial line scan with three fiber components. (a) The experimental setup, (b) and (c) MM–WDM, (d) and (e) SM–WDM, and (f) and (g) PM–PCF.

Fig. 4. Hence, this critical band can be avoided by higher carrier frequencies, typically well above 1 kHz.

In summary of the polarization study, we can conclude that the PM–PCF shows the necessary properties to feed a stable polarization sensitive interferometer system if measures for additional vibration (e.g. sound) protection are taken and AC–based detection schemes are used. The non–polarization maintaining WDMs show less convincing properties. The SM–WDM preserves a certain degree of polarization. Its magnitude and the polarization orientation, however, is significantly influenced by moderate external disturbance. This leads to unfavorable amplitude variations and thereby, potentially to phase misinterpretation. It should be noted that we looked for commercial polarization–maintaining WDMs as substitutes. Nevertheless, existing products are limited by the cut–off wavelength of the fiber for polarization–maintaining emission. The mechanism leading to the unwanted amplitude variations after the SM–WDM is less pronounced for beams emitted by a MM–WDM. The greater isotropy of the polarization distribution in this case mitigates this effect considerably.

## IV. Wavefront Quality

The quality of the emitted wavefronts is a second important parameter for the applicability of the superposed beams. We use a camera beam profiler (CinCam CMOS 1201–Pico, Cinogy) to image the wavefronts and to evaluate the beam profile of both colors. The active area of this sensor is given by the manufacturer with 5.7 mm × 4.3 mm, and the number of the pixel by 2560 × 1920. We use an exposure time of 20 ms. The observed two–dimensional beam profiles for the three fiber components are shown in Fig. 5 together with equatorial line scans. The multi–mode transmission distorts the wavefront of both transmitted colors completely. In case of the SM–WDM the emitted modes are better identifiable in both colors. Nevertheless, substantial noise can be observed in the cross–sections. The 532 nm beam traverses the 1064 nm single–mode fiber in the output of this WDM. Despite the limited length of this fiber, higher spatial modes are populated in the 532 nm beam and increase the noise. In the case of the 1064 nm, however, the spatiotemporal wavefront image shows significantly fewer speckles, but spatial fringes. We attribute these to aperture diffraction at the RC–08 reflective collimator used for these experiments. For the 1064 nm beam, this collimator's NA does not perfectly match the fiber aperture. This can also be observed for the wavefront of the 1064 nm beam from the PM–PCF. In case of the 532 nm beam,

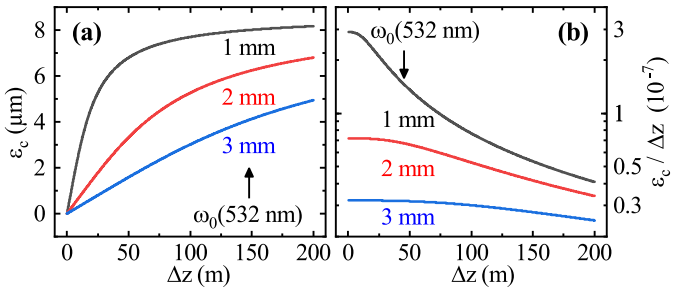


Fig. 6. Absolute (a) and relative (b) chromaticity error induced by the wavelength-dependent numerical aperture of the PM–PCF modeled for a 532/1064 nm two–color interferometer.

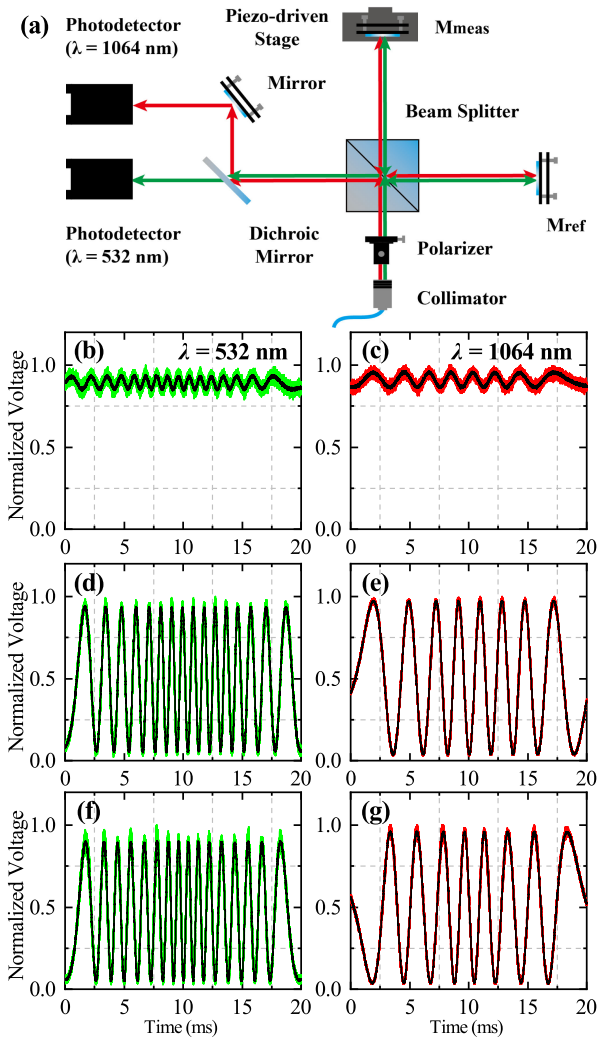


Fig. 7. The interference fringes in coherence measurement with three fiber components. (a) The experimental setup, (b) and (c) with MM–WDM, (d) and (e) with SM–WDM, and (f) and (g) with PM–PCF.

however, the speckle density is greatly reduced compared to the SM–WDM case. According to this, the PM–PCF indeed realizes single-mode transmission for both two–color beams.

The comparison of Fig. 5(f) and (g) further shows a large difference between the beam waists $\omega_0$ of the two wavelengths. Since the reflective collimator ensures equal focal lengths for both colors, this chromaticism is solely introduced by the known strong wavelength–dependence of the NA for PCFs [40]. The NA for 1064 nm is 0.22, for 532 nm only 0.14. If a two–color interferometer uses a PM–PCF fiber to superpose the two beams, the beam waist ratio $\alpha = \omega_0(\lambda_2)/\omega_0(\lambda_1)$ of the two colours $\lambda_1$ and $\lambda_2$ is hence fixed for the complete experiment and determined by the fibers' NAs for these colors, i.e. $\alpha = \mathrm{NA}(\lambda_2)/\mathrm{NA}(\lambda_1)$. It is necessary to investigate the impact of the fixed chromatic beam waist relation on the measurement accuracy of such a two–color interferometer. The absolute magnitude of this effect depends on the detailed optical set-up. However, one can estimate the magnitude with a simple Gaussian beam model. The different beam waists result in divergent propagation wavefronts of the beams. The finite curvature of a Gaussian beam leads to the so–called diffraction error in length interferometry $\varepsilon_{\mathrm{diff}}$ for a optical path difference $\Delta z$. It is given by [41, chpt. 9.3.1.2]

$$\epsilon_{\mathrm{diff}}(\lambda) = -\frac{\lambda}{2\pi} \times \tan^{-1}\left[\frac{\Delta z}{2 z_{\mathrm{R}}(\lambda)}\right] \tag{4}$$

with the Rayleigh length $z_{\mathrm{R}}(\lambda)$ defined as $z_R(\lambda) = \pi\omega_0^2/\lambda$. The chromaticity error $\epsilon_{\mathrm{c}}$ for the two–color interferometer is given by the difference of the diffraction errors of the two colors, scaled up by the $A$-factor:

$$\varepsilon_{\mathrm{c}} = A \times \left(\epsilon_{\mathrm{diff}}\left(\lambda_2\right) - \epsilon_{\mathrm{diff}}\left(\lambda_1\right)\right). \tag{5}$$

Inserting $\lambda_2 = 2\lambda_1$ in the two–color problem and $z_{\mathrm{R}}(\lambda_2) = \frac{\alpha^2}{2} z_{\mathrm{R}}(\lambda_1)$ for the PM–PCF beam waist ratio chromaticism, the chromatic error can be expressed by

$$\varepsilon_{\mathrm{c}} = -\frac{A\lambda_1}{2\pi}\left(\tan^{-1}\left[\frac{\Delta z}{2 z_{\mathrm{R}}(\lambda_1)}\right] - 2\tan^{-1}\left[\frac{\Delta z}{\alpha^2 z_{\mathrm{R}}(\lambda_1)}\right]\right). \tag{6}$$

For a counting 532/1064 nm two-color interferometer the $A$ factor is approximately 65. In Fig. 6 the resulting absolute and relative chromatic errors for beam waists of 1 mm, 2 mm and 3 mm for $\lambda_1 = 532$ nm are depicted. To keep the relative error $\varepsilon_{\mathrm{c}}/\Delta z$ safely below a critical magnitude in refractivity compensation of $1 \times 10^{-7}$, a beam waist larger than 2 mm for the 532 nm beam needs to be worked with. Hence, this effect should be considered in the design of such an interferometer. The beam waist chromaticity uncertainty contribution is probably smaller for the MM–WDM–based combination as it achieves the most homogeneous spatial overlap according to Fig. 5.

## V. Coherence

The most critical beam property for the interferometric application is the degree of coherence remaining after fiber transmission. To study this, we set up a simple Michelson–interferometer following the output polarizer (Fig. 6(a)). The measurement path is modulated by a piezo stage at a frequency of 20 Hz. Measurement and reference beams interfere in the neutral beam splitter. A dichroic mirror (DMSP805, Thorlabs) is used to divide the beams by wavelength and the interference signals are then detected by two photodetectors (HCA–S–200M–SI and HCA–S–200M–IN, FEMTO). The 532 nm and 1064 nm interference signals are simultaneously recorded by an oscilloscope

TABLE III
THE INTERFERENCE CONTRAST OF COHERENCE FRINGES

| Components | $\lambda$ = 532 nm | $\lambda$ = 1064 nm |
|---|---|---|
| MM–WDM | 0.0584 | 0.0578 |
| SM–WDM | 0.8994 | 0.9287 |
| PM–PCF | 0.8998 | 0.9296 |

(SDS1104X–E, SIGLENT) with a sampling rate of 2.5 MSa/s, a memory depth of 70 kpt, and bandwidth of 20 MHz. The observed interference fringes are presented in Fig. 6, the derived interference contrasts $k$,

$$k = \frac{I_{\max} - I_{\min}}{I_{\max} + I_{\min}}, \tag{7}$$

in Table III. For the determination of the interference contrast, the signals were low–pass filtered by a moving average and maximum and minimum voltages $I_{\max}$ and $I_{\min}$ determined. The observed interference contrasts are given in Table III. Due to the short path lengths, this experiment is not designed to study refractive–index compensation and the compensated length is hence not discussed here. In case of the MM–WDM, the interference contrast breaks down almost completely. The distorted wavefronts obviously imply in this case a significant loss of spatial coherence. The signal–to-noise–ratio of an interferometer fed by such a fiber is significantly reduced. SM–WDM and PM–PCF, on the other hand, show similarly high degrees of interference contrast. This is in agreement with the quality of the wavefronts discussed in Section IV and makes them suitable candidates for feeding interferometer heads.

## VI. CONCLUSION

In this paper, three commercial fiber components, an MM–WDM, an SM–WDM, and an endlessly single–mode PM–PCF, are investigated for the combination of harmonic laser beams at 532 nm and 1064 nm. All of the approaches have advantages and disadvantages. Highest–efficiency transmission is realized by the MM–WDM due to its large acceptance angle. The multi–mode transmission induces speckles in this case. As a consequence, the beam wavefronts and coherence are substantially distorted. Additional compensation mechanisms, such as spinning diffusers, might improve the beam profiles for further applications. The SM–WDM could realize a high–contrast interference for both two–color beams, despite considerable speckles at the harmonic due to the transmission below the SM transmission cut–off wavelength. However, current commercially available SM-WDM are unfit for beam combination for polarization-sensitive applications. Mechanical disturbances would induce considerable rotation of the polarization orientation and thus, would lead to misinterpretation of the observation. Finally, the PM–PCF can combine the two–color beams with satisfactory efficiency, maintaining polarization and coherence. But measures need to be taken to cope with this fiber type's distinct NA chromaticity, and, possibly, for proper vibration isolation in polarization–sensitive applications. Since these are no major technical obstacles, beam superposition by PCF fibers seems a very promising option for broadband multi–wavelength interferometry in future.

## ACKNOWLEDGMENT

The authors would like to thank T. Holm for fruitful discussions about the PM-PCFs from NKT Photonics, and T. Meyer and D. Fiala for technical support.

## REFERENCES

[1] W. Gao *et al.*, "Measurement technologies for precision positioning," *CIRP Ann.*, vol. 64, no. 2, pp. 773–796, 2015.
[2] Y. Bock and D. Melgar, "Physical applications of GPS geodesy: A review," *Rep. Prog. Phys.*, vol. 79, no. 10, Aug. 2016, Art. no. 106801.
[3] W. Estler, K. Edmundson, G. Peggs, and D. Parker, "Large-scale metrology–An update," *CIRP Ann.-Manuf. Technol.*, vol. 51, no. 2, pp. 587–609, 2002.
[4] N. Bobroff, "Recent advances in displacement measuring interferometry," *Meas. Sci. Technol.*, vol. 4, no. 9, pp. 907–926, Sep. 1993.
[5] Y.-S. Jang and S.-W. Kim, "Compensation of the refractive index of air in laser interferometer for distance measurement: A review," *Int. J. Mach. Tool. Manuf.*, vol. 18, no. 12, pp. 1881–1890, Dec. 2017.
[6] F. Pollinger, "Interferometry in air with refractive index compensation," in *Modern Interferometry for Length Metrology, ser.* 2053–2563, 2018, pp. 5–1 to 5–42.
[7] J. C. Owens, "Optical refractive index of air: Dependence on pressure, temperature and composition," *Appl. Opt.*, vol. 6, no. 1, pp. 51–59, Jan. 1967.
[8] K. B. Earnshaw and E. N. Hernandez, "Two-laser optical distance-measuring instrument that corrects for the atmospheric index of refraction," *Appl. Opt.*, vol. 11, no. 4, pp. 749–754, Apr. 1972.
[9] K. Meiners-Hagen and A. Abou-Zeid, "Refractive index determination in length measurement by two-colour interferometry," *Meas. Sci. Technol.*, vol. 19, no. 8, Jul. 2008, Art. no. 084004.
[10] K. Minoshima, K. Arai, and H. Inaba, "High-accuracy self-correction of refractive index of air using two-color interferometry of optical frequency combs," *Opt. Exp.*, vol. 19, no. 27, pp. 26 095–26 105, Dec. 2011.
[11] G. Wu, M. Takahashi, K. Arai, H. Inaba, and K. Minoshima, "Extremely high-accuracy correction of air refractive index using two-colour optical frequency combs," *Sci. Rep.*, vol. 3, May 2013, Art. no. 1894.
[12] K. Meiners-Hagen, A. Bošnjakovic, P. Köchert, and F. Pollinger, "Air index compensated interferometer as a prospective novel primary standard for baseline calibrations," *Meas. Sci. Technol.*, vol. 26, no. 8, Jul. 2015, Art. no. 084002.
[13] K. Meiners-Hagen, T. Meyer, G. Prellinger, W. Pöschel, D. Dontsov, and F. Pollinger, "Overcoming the refractivity limit in manufacturing environment," *Opt. Exp.*, vol. 24, no. 21, pp. 24 092–24 104, Oct. 2016.
[14] K. Meiners-Hagen, T. Meyer, J. Mildner, and F. Pollinger, "SI-traceable absolute distance measurement over more than 800 meters with sub-nanometer interferometry by two-color inline refractivity compensation," *Appl. Phys. Lett.*, vol. 111, no. 19, Nov. 2017, Art. no. 191104.
[15] H. Wu, F. Zhang, T. Liu, J. Li, and X. Qu, "Absolute distance measurement with correction of air refractive index by using two-color dispersive interferometry," *Opt. Exp.*, vol. 24, no. 21, pp. 24 361–24 376, Oct. 2016.
[16] H. J. Kang, B. J. Chun, Y.-S. Jang, Y.-J. Kim, and S.-W. Kim, "Real-time compensation of the refractive index of air in distance measurement," *Opt. Exp.*, vol. 23, no. 20, pp. 26 377–26 385, Oct. 2015.
[17] T. A. Birks, J. C. Knight, and P. S. J. Russell, "Endlessly single-mode photonic crystal fiber," *Opt. Lett.*, vol. 22, no. 13, pp. 961–963, Jul. 1997.
[18] A. Ferrando, E. Silvestre, P. Andrés, J. J. Miret, and M. V. Andrés, "Designing the properties of dispersion-flattened photonic crystal fibers," *Opt. Exp.*, vol. 9, no. 13, pp. 687–697, Dec. 2001.
[19] K. Tajima, J. Zhou, K. Nakajima, and K. Sato, "Ultralow loss and long length photonic crystal fiber," *J. Lightw. Technol.*, vol. 22, no. 1, pp. 7–10, Jan. 2004.
[20] K. Nakajima, J. Zhou, K. Tajima, K. Kurokawa, C. Fukai, and I. Sankawa, "Ultrawide-band single-mode transmission performance in a low-loss photonic crystal fiber," *J. Lightw. Technol.*, vol. 23, no. 1, pp. 7–12, Jan. 2005.
[21] K. Ieda, K. Kurokawa, K. Tajima, and K. Nakajima, "Visible to infrared high-speed WDM transmission over PCF," *IEICE Electron. Exp.*, vol. 4, no. 12, pp. 375–379, Jun. 2007.

[22] K. Nakajima, T. Matsui, K. Kurokawa, K. Tajima, and I. Sankawa, "High-speed and wideband transmission using dispersion-compensating/managing photonic crystal fiber and dispersion-shifted fiber," *J. Lightw. Technol.*, vol. 25, no. 9, pp. 2719–2726, Sep. 2007.
[23] K. Kurokawa, K. Nakajima, K. Tsujikawa, T. Yamamoto, and K. Tajima, "Ultra-wideband transmission over low loss PCF," *J. Lightw. Technol.*, vol. 27, no. 11, pp. 1653–1662, Jun. 2009.
[24] T. Matsui, T. Sakamoto, K. Tsujikawa, S. Tomita, and M. Tsubokawa, "Single-mode photonic crystal fiber design with ultralarge effective area and low bending loss for ultrahigh-speed WDM transmission," *J. Lightw. Technol.*, vol. 29, no. 4, pp. 511–515, Feb. 2011.
[25] P. Jamatia, T. S. Saini, A. Kumar, and R. K. Sinha, "Design and analysis of a highly nonlinear composite photonic crystal fiber for supercontinuum generation: Visible to mid-infrared," *Appl. Opt.*, vol. 55, no. 24, pp. 6775–6781, Aug. 2016.
[26] S. K. Varshney, T. Fujisawa, K. Saitoh, and M. Koshiba, "Design and analysis of a broadband dispersion compensating photonic crystal fiber raman amplifier operating in S-band," *Opt. Exp.*, vol. 14, no. 8, pp. 3528–3540, Apr. 2006.
[27] M. De, T. K. Gangopadhyay, and V. K. Singh, "Prospects of photonic crystal fiber as physical sensor: An overview," *Sensors*, vol. 19, no. 3, Jan. 2019, Art. no. 464.
[28] B. H. Lee, J. B. Eom, J. Kim, D. S. Moon, U.-C. Paek, and G.-H. Yang, "Photonic crystal fiber coupler," *Opt. Lett.*, vol. 27, no. 10, pp. 812–814, May 2002.
[29] L. R. Jaroszewicz, K. A. Stasiewicz, P. Marć, and M. Szymański, "Broadband photonic crystal fiber coupler with polarization selection of coupling ratio," in *Proc. 4th Eur. Workshop Opt. Fibre Sensors*, vol. 7653, 2010, Art. no. 76533 W.
[30] K. Grobe and M. Eiselt, *Wavelength Division Multiplexing: A Practical Engineering Guide*. Hoboken, NJ, USA: Wiley, 2013.
[31] C. M. Lawson, P. M. Kopera, T. Y. Hsu, and V. J. Tekippe, "In-line single-mode wavelength division multiplexer/demultiplexer," *Electron. Lett.*, vol. 20, no. 23, pp. 963–964, Nov. 1984.
[32] G. E. Keiser, "A review of WDM technology and applications," *Opt. Fiber Technol.*, vol. 5, no. 1, pp. 3–39, Jul. 1999.
[33] L. Zhang and S. R. Patterson, "Optical mixing errors in a fiber-optic coupled heterodyne interferometer," in *Proc. 17th Annu. ASPE Meeting St. Louis*, 2002, vol. 10, no. 11, pp. 12–13.
[34] S. Cosijns, H. Haitjema, and P. Schellekens, "Modeling and verifying non-linearities in heterodyne displacement interferometry," *Precis. Eng.*, vol. 26, no. 4, pp. 448–455, 2002.
[35] B. Knarren, "Application of optical fibres in precision heterodyne laser interferometry," Ph.D. dissertation, Eindhoven Univ. Technol., Eindhoven, The Netherlands, Jun. 2003.
[36] E. Collett, *Field Guide to Polarization*. Bellingham, WA, USA: SPIE, 2005.
[37] M. Saito, Y. Sato, K. Ikeuchi, and H. Kashiwagi, "Measurement of surface orientations of transparent objects by use of polarization in highlight," *J. Opt. Soc. Amer. A*, vol. 16, no. 9, pp. 2286–2293, Sep. 1999.
[38] A. Dubra and J. A. Ferrari, "Precise polarization measurements using polarizing sheets," *Appl. Opt.*, vol. 37, no. 34, pp. 8156–8157, Dec. 1998.
[39] X. Wang and Z. Wang, "Self-aligning polarization strategy for making side polished polarization maintaining fiber devices," *Opt. Exp.*, vol. 18, no. 1, pp. 49–55, Jan. 2010.
[40] N. A. Mortensen, J. R. Folken, P. M. W. Skovgaard, and J. Broeng, "Numerical aperture of single-mode photonic crystal fibers," *IEEE Photon. Technol. Lett.*, vol. 14, no. 8, pp. 1094–1096, Aug. 2002.
[41] B. Andreas and C. Weichert, "Picometre level displacement interferometry," in *Modern Interferometry for Length Metrology, ser.* 2053–2563. Bristol, U.K.: IOP, 2018, pp. 9–1 to 9–46.

**Yang Liu** received the B.S. degree in mechanical engineering and automation from North China Electric Power University, Beijing, China, in 2014. Since 2014, he has been working toward the M.S. and Ph.D. degrees in instrument science and technology with Tianjin University, Tianjin, China. He is currently on a scientific visit at PTB, Braunschweig, Germany. His research interests include distance measurement with pulse–to–pulse interferometry, as well as refractive–index compensation with two-color interferometry.

**Anni Röse** studied physics in Göttingen, Germany. She received the M.S. degree from the Georg-August University, Göttingen, Germany, in 2018. Since 2019, she has been working toward the Ph.D. degree in mechanical engineering with the Ilmenau University of Technology, Ilmenau, Germany, and is a part of working group 5.42 "Multiwavelength interferometry for geodetic lengths" with PTB. She currently develops a volume–resolved optical thermometer based on two-color interferometry.

**Günther Prellinger** studied physics in Braunschweig, Germany. He received the diploma degree from the Technical University of Braunschweig, Braunschweig, Germany, in 1987. Since 2011, he has been a Member of the PTB working group 5.42 "Multiwavelength interferometry for geodetic lengths." He has developed several approaches to absolute distance interferometry for applications in precision engineering.

**Paul Köchert** studied control engineering in Ilmenau, Germany. He received the doctoral degree from the Ilmenau University of Technology, Ilmenau, Germany, in 2018. He has worked at the TU Ilmenau and PTB, since 2009 and is now working in the PTB working group 5.42 "Multiwavelength interferometry for geodetic lengths." His research interests concentrate on the development of FPGA-based system for displacement measuring interferometry and laser standards.

**Jigui Zhu** received the M.S. degree from the National University of Defense Technology, Changsha, China, in 1994, and the Ph.D. degree from Tianjin University, Tianjin, China, in 1997. He is currently a Professor with the College of Precision Instrument and Opto–Electronics Engineering, Tianjin University. In April 2016, he was appointed the Changjiang (Yangtze River) Scholar Distinguished Professor by the Ministry of Education, China. His current research interests include laser and optoelectronic measuring technology, large-scale dimensional metrology, and online vision inspection.

**Florian Pollinger** studied physics in Würzburg, Germany, and Austin, TX, USA. He received the doctoral degree from the University of Würzburg, Würzburg, Germany, in 2009. He then joined PTB and has been leading the PTB working group 5.42 "Multiwavelength interferometry for geodetic lengths" since 2010. He is also currently coordinating the EMPIR JRP "Large–scale dimensional measurements for geodesy" (GeoMetre). His research focuses on fundamentals and applications of multiwavelength interferometry for the SI–traceable length measurement on large scales with low measurement uncertainty.